A Robot System for Automated Wound Filling with Jetted Materials

Bashir Hosseini Jafari, Lee Namhyung, Rachael Thompson, Jackson Schellhorn,
Bogdan Antohe and Nicholas Gans

***Abstract*— Skin surface wounds due to burns, surgeries and chronic illness affect millions of people worldwide. Tissue engineering has become an increasingly popular treatment, but it is a highly manual process. Increasing the automation in tissue engineering could increase the rate of treatment for patients and improve outcomes. We present an initial investigation into an automated in-situ treatment. In our proposed method, a 3D machine vision system detects a skin wound to be treated and then determines the 3D point set corresponding to the wound. The 3D point set is then passed to path planning algorithm for a robot manipulator to move an ink-jet nozzle over the wound and fill the cavity with quick-curing/gelling fluids such collagen and other biomaterials and cell growth promoters. This paper details initial results and experimental validation of each of the proposed steps.**

I. Introduction

Each year in the United States there are an estimated 500,000 people treated for burn injuries, with more than 40,000 requiring hospitalization [1]. More than 3.5 million people are treated for skin cancer each year, with surgical excising and cauterization being the most common treatment [2]. Chronic wounds have also become an issue for millions of people [3], [4]. Tissue Engineering has emerged as a major treatment option [5]. Tissue engineering includes growing living tissue for implantation or creating structures of nonliving biomaterial that encourages cell growth by the patient. In either case, the process is highly manual, with medical experts measuring the wound [6], then designing and often building the tissue or engineered structure by hand.

This paper presents an initial investigation into automated treatment options for wounds using robot systems. These treatments can be highly individual, as the depth of the wound varies and can be more precisely controlled to better match curvature compared to conventional bolus methods. Ultimately, we can deposit growth factor regulators, cell buffers, and bio-absorbable collagen scaffolds before the cavity is filled with collagen. Patients will thus benefit through improved recovery defined by quicker healing, better functionality and aesthetics with less cost, pain and suffering. An automated approach will potentially offer a number of advantages over manual deposition. A robot can perform more precise and repeatable placement. For treatments like cell seeding, a structural material such a collagen is placed in layers, and cell solutions are regularly spaced through the filler. Accurate placement of cell solution leads to much better results, necessitating greater accuracy than by hand. Deposited materials are often placed in specific patterns, such as to promote nerve growth connecting a severed nerve. An automated approach to extract the position and orientation of the wound will allow precise placement even given patient motion between deposition of materials and cells solutions. Furthermore, uniform placement of filler material is made easier by maintaining a constant speed for robot end-effector, leading to accurate layering.

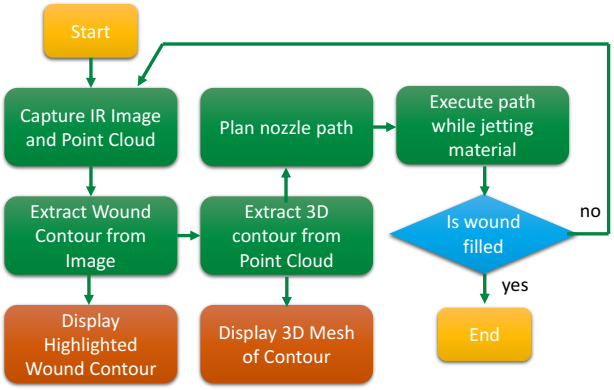

Fig. 1. Diagram of the wound treatment process.

There have been some recent related works on automated wound treatment, including using liquid-jet or deposition technologies. A comparison of manual and automated wound measurement techniques was presented in [7]. A good review of work on the topic of bioprinting can be found in [8]. In terms of combining automating wound detection and bioprinting, [9] presented image processing algorithms for extracting the closed-boundaries of wounds, which are then used to define a shape sent to a bio-printer ex situ. Wound depth is not considered, but the authors note several ways to do so in the future. For in situ treatments, the authors of [10] propose a high-pressure water jet to cut or abrade tissue. They present path planning and robot kinematics to guide the jet along the desired path over the tissue. Direct printing of liquids onto a moving limb was demonstrated in [11], which moved the print-head to compensate for detected motions of the limb that was tracked using stereo vision and laser rangin. Printing on a human-limb using fiducial markers for vision-based localization was also presented in [12]. Neither of these systems included vision to extract a wound or other

This material is based upon work supported by the National Science Foundation under Grant No. 1563424

B. Jafari, L. Namhyung, and N. Gans are members of the Department of Electrical and Computer Engineering; J. Schellhorn is a member of the Department of Mechanical Engineering; The University of Texas at Dallas, Richardson, TX 75080, USA. R. Thompson is with Plano West High School, Plano, TX. B. Antohe is with Microfab Technologies Inc., Plano, TX {bxh140430, nxl160830, sjs170330, ngans}@utdallas.edu; bogdan.antohe@microfab.com .

region and conduct motion planning.

In contrast to these efforts, we present the initial investigation into a end-to-end system for automated wound detection and in situ tissue printing. That is, we extract the position and shape of the wound, plan a path for the print-head, then directly jet material onto the wound in desired patterns and proportions to provide level filling of the wound. This liquid will ultimately be replaced with collagen and/or hydrogel solutions that can be cured/stiffened under a pH change or UV light exposure. The curing will be done after one or more filler layers and is followed by the more accurate deposition of cells or other functional materials.

In our proposed system, the first step uses a 3D vision system to extract the wound boundary using visual cues and features. We then determine a 3D set of points corresponding to the wound, providing a point cloud. The contour of the wound is extracted as a 3D closed curve, and this set of points is used to determine a path for a robot-guided valve-jet nozzle to dispense fluid. The fluid is cured using UV light to a stiff gel. The process iterates until the wound is filled. The process is illustrated in Fig. 1. The major contribution of this work is demonstration of the first end-to-end process for automated wound filling (to our knowledge). Each step of which has been experimentally verified for a variety of wound shapes and motion patterns.

The paper proceeds as follows. Section II describes the 3D vision system, the vision algorithms to detect the wound and extract the 3D point set. Section III describes how the 3D wound contour is used to determine a path for the robot to move and guide the jet nozzle. Section IV presents the final experimental results for end-to-end runs of the proposed approach. Finally, in Section V, we provide conclusions and discuss plans for future work.

II. Vision System For Wound Contour Extraction

Our vision system is based around an Ensenso N35 3D camera by Image Development Systems. The Ensenso uses a stereo-pair of near infrared (IR) cameras with an IR projector to generate a dot pattern. The stereo cameras use the dot pattern to provide texture for matching points in the two images. Both projector and cameras operate at approximately 850nm wavelength. The result is a $1280 \times 1024 \times 3$ point cloud (i.e. approximately 1 million points in $\mathbb{R}^3$). At a standoff distance of approximately 0.5m from a target, the point cloud depths are accurate to about 0.5mm. For comparison, the wound resulting from a melanoma removal can 8-10mm deep [13] and severe burns can be up to 3mm in depth. The camera calibration program provided by Enenso enables registration of the point cloud to a 3D location using a calibration board. This let us specify the reference frame in which the point cloud coordinates are returned to have origin at a known point in the robot work space and axes aligned with the robot's base frame axes.

Point Cloud Library (PCL) [14] v1.8 interfaces between the Ensenso Camera and Robot Operating System (ROS) [15]. PCL delivers the point cloud as well as the IR images

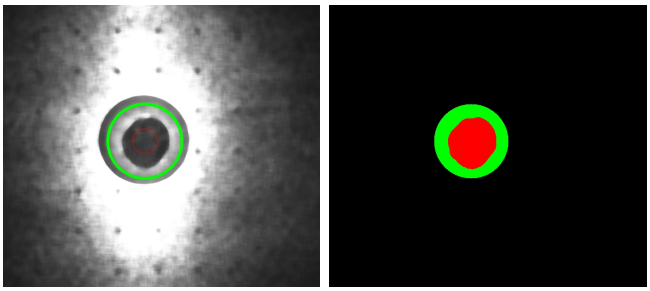

Fig. 2. (Left) The smoothed IR image with a wound contour identified. Red and green circles are drawn in indicate the interior and exterior regions. (Right) The red region is the determined wound region to be treated, and green region is surrounding non-wound regions to aid in visualization.

for image processing using OpenCV [16]. The IR images are processed to automatically find a wound region. Blob detection is carried out in the left IR image, as Ensenso uses the optical center of the left camera to define the origin of the point cloud. The IR image is noisy due to the IR projector, so we conduct a round of Gaussian and median smoothing. The loss of texture and features is not punitive for the task of blob detection. Coplanar points corresponding to the table surface below the 3D object can be removed from the point cloud, and the remaining surface points used to estimate a region of interest for the search of the wound contour.

In this preliminary work, we use white foam objects with "wounds" carved out. The wounds are colored with ink that shows up dark under near IR frequencies. Blob detection is carried out using OpenCV. The contour of each blob is then extracted, and the set of contours is reduced based on appearance and characteristics of the contour. Specifically, the intensity of the contour interiors must be below a specified level, indicating the wound is suitably dark. Area must be suitably large, in our case over 5000 pixels. The convexity of the wounds and ratio of horizontal and vertical inertia (i.e. circularity) is used to reduce the number of detected candidate wounds, as can other contour moments or functions of moments [17]. Future work will focus on registering the point cloud to an RGB camera to conduct more advanced wound detection and extraction using color images [9].

After determining the region of interest and eliminating specious contours, the IR image is displayed with the final contours and wound interiors indicated for the user to approve. This is shown in Fig. 2 (left), with a target consisting of a hemispherical foam shape that has had an irregular wound carved out. A red circle indicates the extracted wound. A green circle indicates the region of interested corresponding to non-coplanar points in the point cloud.

After a user approves the wound to be treated, the 3D contour of the wound is determined. There is a one-to-one correspondence between pixels in the left IR image and points in the point cloud. Therefore, using the detected wound contour in the IR image, we can extract the set of 3D points that correspond to the wound. If desired, a set of points outside the wound can also be extracted to help a user visualize the wound. The number of points on the wound interior is typically very large (on the order of 10,000-50,000

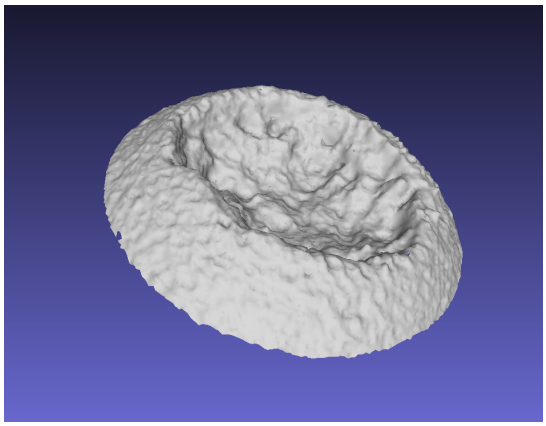

Fig. 3. The extracted point cloud of a hemisphere with a wound, including the surrounding area, converted to a mesh.

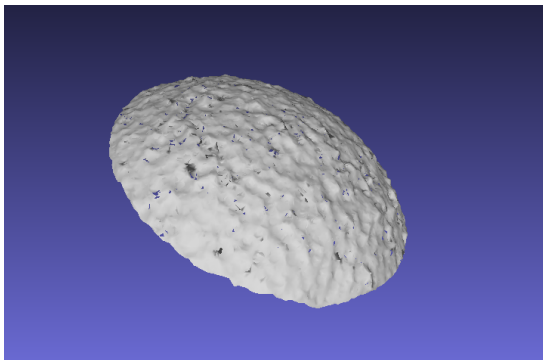

Fig. 4. The extracted point cloud of a hemisphere without a wound, converted to a mesh.

points). Therefore, just the points of the contour edge are kept, consisting of a set of N points with coordinates

$$p_k = [x_k,\, y_k,\, z_k]^T, \quad k \in 1 \ldots N. \tag{1}$$

This set of 3D points is then sent to the robot path-planning algorithm.

Fig. 2 (right) shows the precise contour and surrounding region of the previous example, which is then extracted from the point cloud. The corresponding set of points is seen in Fig. 3, where the point cloud has been converted to a mesh for easier visualization. The general hemispherical shape and carved wound are clearly visible. For comparison, Fig. 4 shows a hemisphere that has not had a wound carved.

III. Robot Motion Planning and Fluid Deposition Control

Automated deposition offers a number of advantages over deposition by hand. A robot can provide more precise and repeatable placement. For treatments like cell seeding, a support or filler material such as collagen or hydrogel is placed, and cell solutions are regularly spaced throughout the filler. Accurate placement of cell solution leads to much better regenerative results, necessitating greater accuracy than by manual deposition. Furthermore, uniform placement of filler is made easier by maintaining a constant speed for robot end-effector, leading to accurate layering.

After the wound contour is extracted from the point cloud, the set of points is used to define a path for the ink-jet nozzle, which, in turn, defines a set of control points for the robot end effector. The robot is a Staubli TX90, with 6 degrees of freedom. A mount for the inkjet nozzle was machined, with the offset from the end effector flange known through the CAD design. Fluid flow from the nozzle is controlled by a solenoid valve and driven by a pulse train generated by an Arduino micro controller, then amplified to the necessary voltages levels. A compressed air tank with a digital regulator provides air pressure to a syringe reservoir filled with liquid. The setup is shown in Fig. 5.

Through the aforementioned calibration routine for the N35, the point cloud is defined with respect to a Cartesian reference frame with origin on the table in front of the robot and aligned with the robot major axes. The origin of this frame is determined in the robot base frame by simply moving the end effector to the origin on the calibration board using the robot teach pendent. The position and orientation of the nozzle can always be determined by the robot's own forward kinematic routines. There is no need for further processing the point cloud to extract the principal axes of the point cloud.

Multiple paths were considered. The simplest is a "lawn mower" or "bricklayer" path consisting of lines back and forth from the edges of the wound. The lines are defined along the robot x-axis, and equally spaced at intervals (e.g., 2mm) along the robot y-axis. The location of the wound edges in the robot work space is provided by the point cloud. The z-coordinate of the path, i.e. the height of the nozzle is held fixed at 6mm above the highest point on the wound contour to ensure no contact with the wound surface. Future work will focus on reducing the height for more precise placement. The orientation of the nozzle is fixed with the nozzle approximately vertical. We also investigated a path that approximates a spiral starting from the wound center and progressively getting larger.

The bricklayer path works well for wounds with a contour that is close to convex. If the wound is highly non-convex, the straight line path will eventually take the nozzle outside the wound contour. These regions can be planned for and jetting halted, but it is possible that some material will end up outside of the wound. The materials are non-toxic, but waste is not desirable. The spiral path works well for both convex and non-convex shapes, as the nozzle always remains within the contour. Additionally, as the filling process must be repeated to deliver multiple layers, the spiral pattern simply requires the end point be moved father along the spiral curve at each iteration. The bricklayer path requires new start and end points at each iteration to gradually fill from the center. Future work will base the paths on the point cloud as well as the contour. For structure and filling it is often preferred to start at the deepest part of the wound, which may not be the center. Wounds with multiple local minima will require more complicated paths, likely the union of multiple curves centered at each minima. Once the minima are filled, the remainder can be addressed with a single curve.

The path planner then determines a set of control points at the end of each line. The robot executes a path through the

control points using the Staubli Val 3 programming language. The robot has a fixed velocity throughout the path in this work. This is an iterative process, with the wound contour being extracted, the path being followed and fluid jetted, then a picture being taken to determine if the wound is filled. The contour can be extracted anew at each iteration in case it has filled in shallow regions. Time can be allowed for the fluid to cure or set, if desired, including a stage of exposing to a UV light source. The process is repeated until the wound is filled to a desired depth. Future work will include multiple stages of printing different materials. This can include printing materials that promote growth of specific cells, such as nerve cells, biomaterial scaffolds, and finally filling material. A polymer bandage can then be applied over the surface to seal it.

The rate of fluid flow from the nozzle is regulated by a PWM signal sent to a solenoid valve. In this work, the duty cycle of the PWM signal is fixed. We have a joint research in adaptive control to regulate line width [18], which will be integrated with this project. A variety of fluids can be jetted with different viscosity and properties. In this work, we used a 25 wt% pluronic F127 (Poloxamer 407) solution with water, which has low viscosity when chilled but turns into a gel at room temperature. Similar solutions can be used that cure under exposure to UV light or exposure to a higher pH solution. Various dyes can be added to the solutions for visualization and inspection. Ultimately, we propose to use a treated hydrogel that cures under UV light. Future work can focus on printing different materials in sequence to place scaffolds, tissue growth conduits and filling material.

We need to stop fluid deposition based on a criteria that can guarantee the wound is almost filled. It is straightforward to estimate the volume of the wound cavity using the point cloud data. Denote fluid volume as V and volume flow rate of the fluid coming out of nozzle as Q. That is $Q = \frac{dV}{dt}$. Given a constant, known Q (which can be predetermined off line as function of valve input duty cycle), the total volume dispensed in time t is $V = Qt$.

Given the point cloud set of the wound contour and interior, the height z of every point can be expressed as a function of the x and y coordinates, i.e. $z = f(x, y)$. The volume of any region of the wound cavity, V_c, can be approximated as

$$V_c = \sum_x \sum_y (z_d - z)\delta x \delta y \tag{2}$$

where z_d is the desired level to which we want to fill the region of the wound in a given iteration, and δx and δy are the displacement along the x and y directions between each point sample. The approximate time to fill the region of the wound cavity to the desired level of that iteration can be calculated as

$$t = \frac{V_c}{Q}. \tag{3}$$

The total path length of the nozzle is known. Therefore, the velocity of the robot can be set to complete the path in time t. Alternately, given a desired robot velocity we can calculate the time to complete the path and set the flow rate.

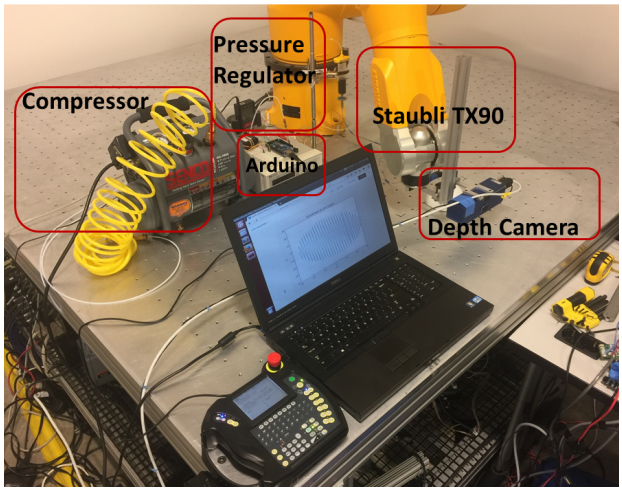

Fig. 5. Experimental Setup.

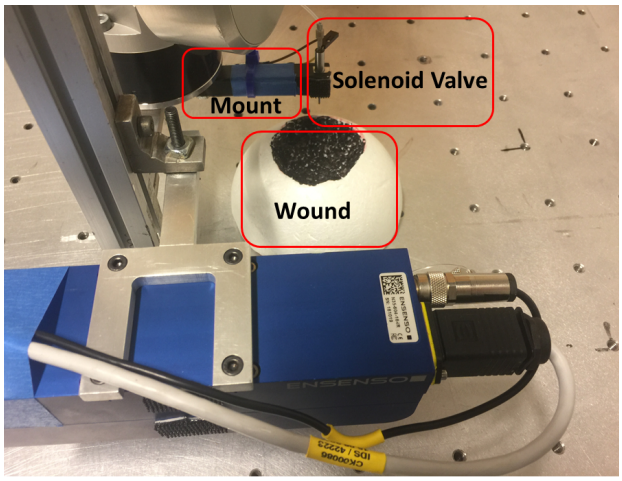

Fig. 6. The camera, wound and valve setup

IV. Experimental Results

In this section, we provide several examples of the end-to-end automated wound treatment process. Our experimental setup can be seen in Fig. 5, with a close up view of the camera, valve/nozzle and wound being treated shown in Fig. 6. The 3D camera is mounted on the end effector of the Staubli robot, and it is held approximately 0.5 meters above the target during imaging. After the image processing, contour extraction and path planning have been executed, the robot moves the nozzle to 6mm above the wound and conducts the planned path while jetting fluid. The camera and valve mounts are designed to prevent accidental contact of the camera with the table or camera mount with the wound.

We first show results for the hemispherical object with wound point cloud seen in Fig. 4. The number of points on the wound interior was almost 20,000, and the contour edge consisted of 221 points. Three paths over the entire wound are presented. The first, shown in Fig. 7 (top-left) consists of a denser set of straight line across the wound. The second,

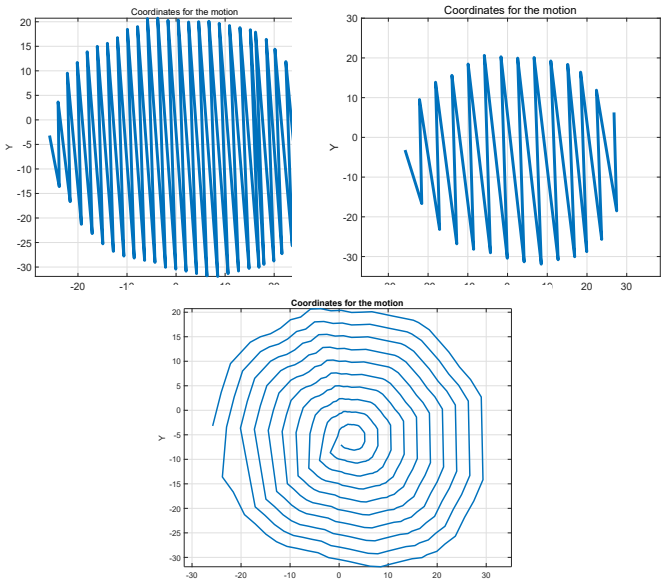

Fig. 7. The high density (lop left) and low-density (top right) line motions and spiral (bottom) motion for the robot end effector for the circular wound.

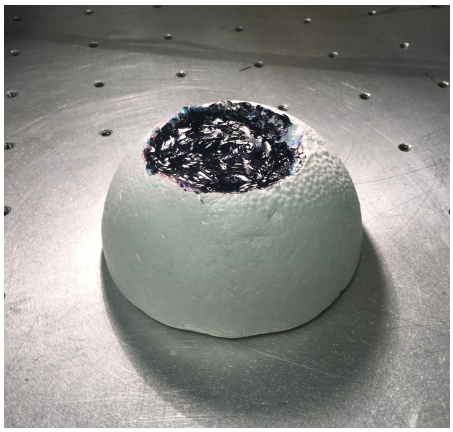

Fig. 8. The hemispherical object with circular wound filled with gel.

shown in Fig. 7 (top-right) has more space between passes. It can be confirmed that the end points of each pass are on the wound edge contour. The third was the spiraling path defined by the contour, shown in Fig. 7 (bottom).

The velocity of the robot end effector was set to 1cm/sec, which is relatively slow to avoid splattering the fluid. For timing, two approaches were considered for each path. The first is to completely fill the wound in one iteration. With t determined by the velocity and path length, the flow rate and duty cycle are then determined by (3). The second approach is to fill the wound in n iterations, with the fluid flow rate set to $\frac{Q}{n}$ compared to the single iteration rate. In this case, the camera is raised, and the wound fill level is checked after each round. The remaining volume and flow rate can be recalculated to add robustness to the process. This also gives time for layers of liquids to set or cure. The final filled circular wound can be seen in Fig. 8. The gelled nature of the fluid can be seen in the texture of the fill. .

We then conducted a more realistic experimental scenario with a wound on a foam head. The wound shape is inspired by a real wound seen in [9]. The IR image with indicated

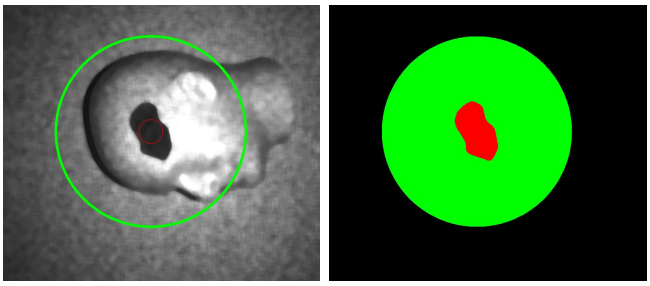

Fig. 9. (Top Left) The smoothed IR image with a wound contour identified. Red and green circles are drawn in indicate the detected wound and nonplanar region of interest. (Top right) The red region is the determined wound region to be treated, and green region is the detected nonplanar region of interest.

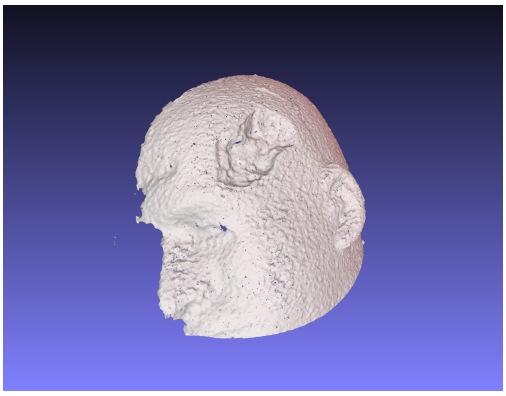

Fig. 10. The extracted point cloud of a head with a wound, including the surrounding area, converted to a mesh.

wound is seen in Fig. 9 (left). The corresponding contour and surrounding region of interest are shown in Fig. 9 (right), with the surrounding region to include more visible features in the point cloud. The contour consisted of 330 points. The mesh of the point cloud is shown in Fig. 10, with the wound clearly visible. The denser and sparser paths and the spiral path over the entire wound are shown in Figs. 11.

We present a final experiment to demonstrate the accuracy and repeatability of our wound filling method and to depict its advantage over manual filling. For the sake of visibility and distinction, a sparse version of spiral pattern in Fig. 11 was printed on paper. A red line was deposited first to simulate a structural or filler layer. A second line, in blue, was then deposited to simulate as a cell solution or cell-growth promoter material. The cell material needs to closely overlap the filler material. Fig. 12 shows four images from the sequence. As can be observed, the lines are accurately applied, with a level of precision outside most manual applications

V. Conclusions and Future Work

Automated tissue engineering has great potential as a treatment for skin wounds, which affect millions of people worldwide. The accuracy and repeatability of a robot system over manual treatment has many advantages in patient outcomes. We have presented an initial investigation into an automated in-situ treatment. First, a 3D machine vision system located wounds based on visual cues and retrieves the 3D point set corresponding to the wound. The point set

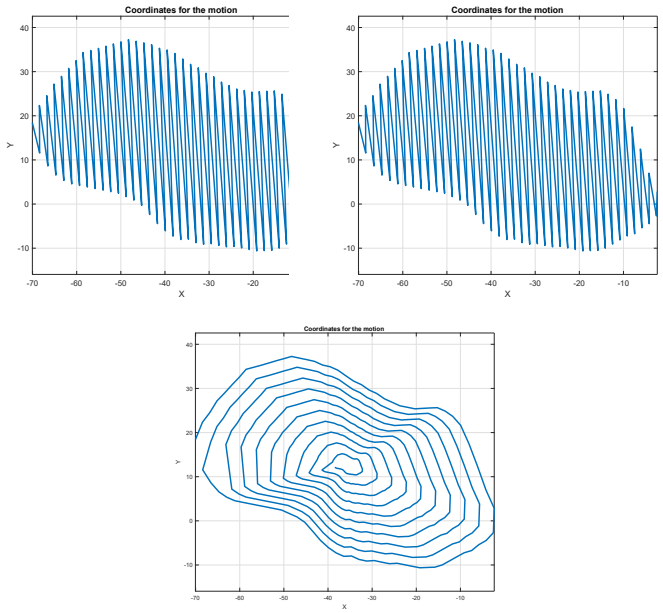

Fig. 11. The high density (lop left) and low-density (top right) line motions and spiral (bottom) motion planned for the robot end effector for the head wound.

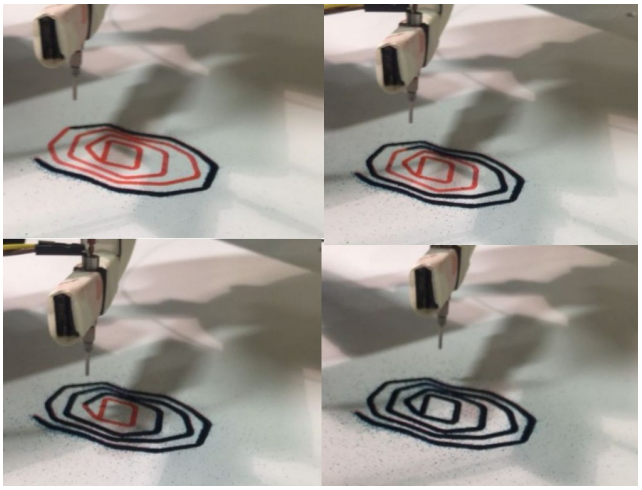

Fig. 12. Accuracy and repeatability verification for the filler and cell solution alignment.

is used to define a path for a robot to guide an ink-jet nozzle over the wound and fill the cavity.

This was an initial investigation of the entire process. Each step in the process will be investigated in much greater detail. The vision algorithms for wound detection were based on detecting dark regions in the image, and will be replaced with more sophisticated algorithms. We are incorporating a color camera registered with the IR stereo cameras, in which case we can use color cues and train the system to find regions that look like raw tissue. The path planning presented was also for a relatively simple task of filling the wound cavity. Ultimately, we want to print biomaterial scaffolds, patterns of materials to promote specific cell growth (e.g. nerve cells along specific printed conduits) and more prior to wound filling. The depth of the wound and local minima must be considered in future path planning as well. Some materials will require a period of curing under UV light, necessitating a robot path to guide a light source between printing rounds. Assuming the region under treatment is immobilized, the motion of the nozzle can largely be performed using open-loop control. However, we are also investigating approaches to closed-loop control to ensure the deposited materials are in the correct locations and amounts.

VI. Acknowledgment

We would like to acknowledge Prof. Ronald Smaldone of the UT Dallas Department of Chemistry for his help in determining and providing appropriate printing materials.

References

[1] "Burn incidence and treatment in the united states: 2013 fact sheet." http://www.ameriburn.org/resources_factsheet.php.

[2] "Skin cancer facts." http://www.skincancer.org/skin-cancer-information/skin-cancer-facts.

[3] I. Rodrigues and M.-F. Mégie, "Prevalence of chronic wounds in quebec home care: an exploratory study," *Ostomy/wound management*, vol. 52, no. 5, pp. 46–8, 2006.

[4] C. K. Sen, G. M. Gordillo, S. Roy, R. Kirsner, L. Lambert, T. K. Hunt, F. Gottrup, G. C. Gurtner, and M. T. Longaker, "Human skin wounds: a major and snowballing threat to public health and the economy," *Wound Repair and Regeneration*, vol. 17, no. 6, pp. 763–771, 2009.

[5] R. A. Clark, K. Ghosh, and M. G. Tonnesen, "Tissue engineering for cutaneous wounds," *Journal of Investigative Dermatology*, vol. 127, no. 5, pp. 1018–1029, 2007.

[6] A. Shah, C. Wollak, and J. Shah, "Wound measurement techniques: comparing the use of ruler method, 2d imaging and 3d scanner," *Journal of the American College of Clinical Wound Specialists*, vol. 5, no. 3, pp. 52–57, 2013.

[7] D. M. Wendland and D. W. Taylor, "Wound measurement tools and techniques: A review," *Journal of Acute Care Physical Therapy*, vol. 8, no. 2, pp. 42–57, 2017.

[8] D. M. Kirchmajer, R. Gorkin III, *et al.*, "An overview of the suitability of hydrogel-forming polymers for extrusion-based 3d-printing," *Journal of Materials Chemistry B*, vol. 3, no. 20, pp. 4105–4117, 2015.

[9] P. Gholami, M. A. Ahmadi-pajouh, N. Abolftahi, G. Hamarneh, and M. Kayvanrad, "Segmentation and measurement of chronic wounds for bioprinting," *IEEE Journal of Biomedical and Health Informatics*, vol. PP, no. 99, pp. 1–1, 2017.

[10] T. Bahls, F. A. Fröhlich, A. Hellings, B. Deutschmann, and A. O. Albu-Schäffer, "Extending the capability of using a waterjet in surgical interventions by the use of robotics," *IEEE Transactions on Biomedical Engineering*, vol. 64, no. 2, pp. 284–294, 2017.

[11] J. J. O'Neill, R. A. Johnson, R. L. Dockter, and T. M. Kowalewski, "3D bioprinting directly onto moving human anatomy," in *IEEE/RSJ International Conference on Intelligent Robots and Systems*, pp. 934–940, 2017.

[12] Z. Zhu, S.-Z. Guo, T. Hirdler, C. Eide, X. Fan, J. Tolar, and M. C. McAlpine, "3d printed functional and biological materials on moving freeform surfaces," *Advanced Materials*, vol. 30, no. 23, p. 1707495, 2018.

[13] H. Pickett, "Shave and punch biopsy for skin lesions," *American family physician*, vol. 84, no. 9, p. 995, 2011.

[14] R. B. Rusu and S. Cousins, "3D is here: Point Cloud Library (PCL)," in *IEEE International Conference on Robotics and Automation (ICRA)*, (Shanghai, China), May 9-13 2011.

[15] M. Quigley, K. Conley, B. Gerkey, J. Faust, T. Foote, J. Leibs, R. Wheeler, and A. Y. Ng, "Ros: an open-source robot operating system," in *ICRA workshop on open source software*, vol. 3, p. 5, 2009.

[16] K. Pulli, A. Baksheev, K. Kornyakov, and V. Eruhimov, "Real-time computer vision with opencv," *Communications of the ACM*, vol. 55, no. 6, pp. 61–69, 2012.

[17] M.-K. Hu, "Visual pattern recognition by moment invariants," *IRE transactions on information theory*, vol. 8, no. 2, pp. 179–187, 1962.

[18] B. Jafari, N. Lee, B. Antohe, and N. Gans, "Parameter estimation and line width control of robot guided inkjet deposition," in *2018 American Controls Conference*, 2018.